A narrowband filter with wide free-spectral-range and independent tunability of transmission coefficients

Feixia Bao, Chang Wang, Shilong Pan, *Fellow, IEEE* and Ang Li, *Member, IEEE*

Abstract—**We present an integrated filter on silicon photonics with wide free-spectral-range and sub-nm bandwidth, which is particularly suitable for programmable photonic circuit with arbitrary spectral responses. The unique feature is that its extinction ratio, namely the transmission coefficient within the bandwidth, can be independently controlled from 0 to 1 without affecting the rest optical span. Thus, a series of such building blocks with varying center wavelengths can be concentrated to form a programmable photonic circuit that can generate arbitrary spectral responses with easy control logic. The notch filter is a Mach-Zenhder-Interferometer with narrowband contra-directional couplers (CDC) and the filter performance is greatly enhanced compared with previous results. The bandwidth is reduced by a factor of 4 and the device length is only one third of previous demonstration.**

Index Terms—**silicon photonics, contra-directional couplers**

I. INTRODUCTION

Integrated filters that can selectively transmit or suppress specific wavelengths are essential components in various fields such as telecommunications, photonic computing, spectral shaping, and optical sensing[1-7]. Having a wide free-spectral-range (FSR) for the filter, which determines its operational bandwidth, and a narrow bandwidth for high spectral resolution is highly desirable. Additionally, the ability to tune the extinction ratio of the filter, namely the transmission coefficient within its bandwidth, would expand its range of applications[8]. Particularly, this kind of device would be a great candidate to develop programmable photonic circuit (PPC) or photonic circuit with arbitrary spectral responses. PPC is an emerging device that can produce arbitrary spectra by programming the internal states of the circuit[9]. Current demonstrations are all based on Mach-Zehnder-Interferometer (MZI) meshes with hundreds of phase shifters (PS)[9-11]. By tuning the PSs, different physical routes between input and output can be formulated, so that varying output spectra can be produced. However, the link between the configurations of those hundreds of PSs and the target spectrum is hidden. Thus, it requires complex control logic to configure those PSs in order to obtain the desired spectrum. and it is time and resource consuming.[12, 13] However, a novel method of creating an PPC with arbitrary response can be built with narrowband filters with the ability to tune the extinction ratio, where the connection between phase shifters and wavelength response is more direct. Modular components, which can tune the transmission coefficient at a single predetermined

wavelength, can be concatenated to allow arbitrary response over a larger spectral bandwidth as shown in Fig. 1. One potential application scenario for such device is to provide various filtering spectra, such as bandpass filter, bandstop filter, low-pas filter, high-pass filter, linear filter etc. Alternatively, it can be used to generate various distinct spectra used for computational spectrometers[14].
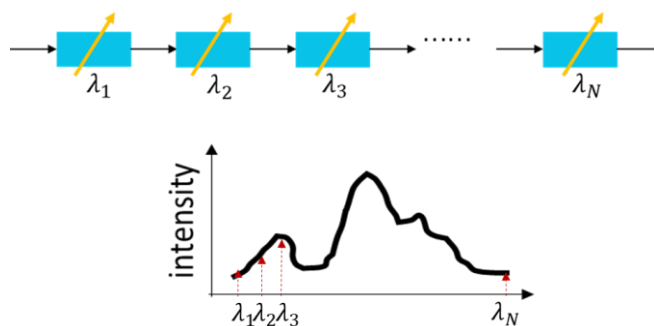

Fig. 1 A novel type of programmable photonic circuit to generate arbitrary spectral responses by cascading a series of building blocks that control the transmission coefficients at specific wavelengths.

resonator modifies the transmission coefficient at center wavelength by changing the coupling coefficient

Conventional integrated filters utilize ring resonators, imbalanced Mach-Zehnder Interferometers (MZIs), Bragg gratings, or photonic crystal cavities. Despite different approaches to increase the FSR and decrease bandwidth, a common problem persists among all these filters - the independent tunability of the extinction ratio, or the transmission coefficient within its bandwidth. In conventional filters, the transmission coefficient within its bandwidth is modified by shifting the operation wavelength[15-17], as depicted in Figure 2(a-c). While this method efficiently modifies the transmission at the desired original wavelength range (λ_0), it also affects the transmissions at other optical span. One potential solution is to use a coupler-tunable ring resonator[3], as illustrated in Figure 2(d). By adjusting the coupling ratio, the extinction ratio of the peak or notch produced by the ring resonator can be modified. However, this approach also alters the bandwidth simultaneously, and it inevitably increases the roundtrip length of the ring resonator,

F. Bao, C. Wang, S. Pan and A. Li are with the National Key Laboratory of Microwave Photonics, Nanjing University of Aeronautics and Astronautics, Nanjing 211106, China (ang.li@nuaa.edu.cn); Ang Li is also with Key Lab of

Modern Optical Technologies of Education Ministry of China, Soochow University, Jiangsu, China

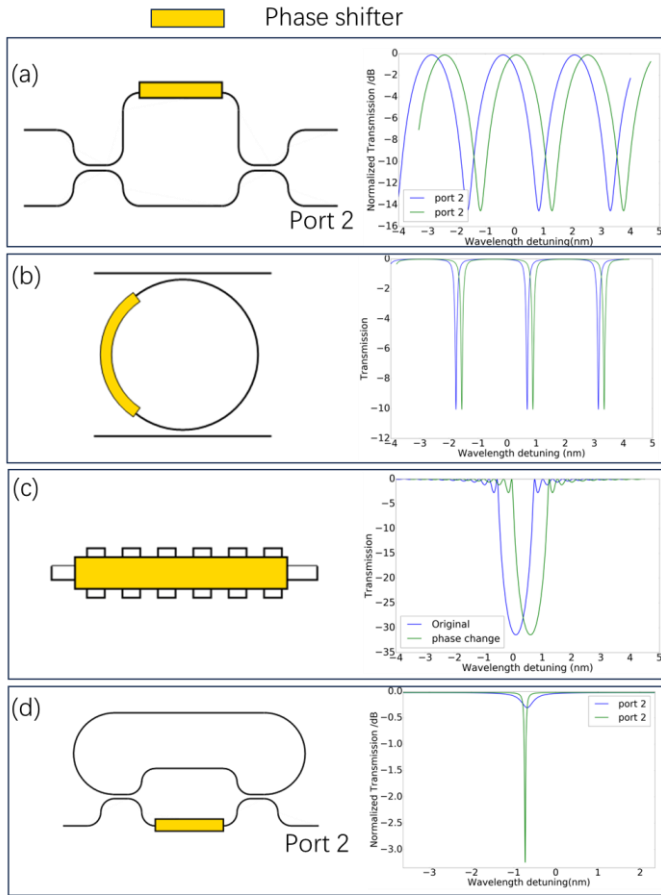imposing a limitation in the achievable FSR

Fig. 2 (a-c) conventional narrowband filters based on MZI, ring resonator and Bragg grating modify the transmission coefficient at center wavelength by shifting the spectrum. (d) Coupler-tunable ring

In a previous study[18], we successfully demonstrated such a narrowband filter with wide FSR and independent tunability of transmission at the center wavelength, while preserving the remaining spectral range. This was achieved by utilizing a MZI with narrowband contra-directional couplers (CDC) instead of conventional directional couplers as depicted in Fig. 3(a). However, there were a few limitations due to the lack of optimization of structural parameters. Firstly, the bandwidth of the filter was over 2nm, which was considered too wide for precise wavelength selectivity. Secondly, the footprint of the filter was relatively large as we're using cladding modulation with weak coupling strength. Thirdly, there exists strong coupling to the reflection mode, as the CDC consists of two identical waveguides. Lastly, the maximum extinction ratio was limited to 15dB as the peak of the CDC deviated from the ideal value of 0.5. To address these limitations, we re-designed the CDC based on two asymmetric waveguides with negligible coupling to the reflection mode and have applied complementary lateral-misalignment modulation to reduce the bandwidth, resulting in enhanced performance of the narrowband filter. As a result, the bandwidth has been reduced to 0.6nm, making it more suitable for telecommunications applications. Additionally, the footprint of the filter has been reduced by a factor of 2. Furthermore, the extinction ratio has been improved to over 22dB.

2. Device design and simulations

Conventional Mach-Zehnder Interferometers (MZIs) typically employ broadband directional couplers as the splitter and combiner. As a result, the interference effect occurs over a wide optical range. When the relative index between the two arms of the MZI is changed, the transmissions across a broad optical range are simultaneously modified. In contrast, narrowband contra-directional couplers (CDC) only couple a limited spectral range to the adjacent waveguide[19, 20]. When CDCs are integrated into an MZI as the splitter and combiner, the interference effect is confined to the narrow passband of the CDC, and the phase change in the MZI only affects the transmission at the center wavelength of that narrow passband.

CDC is a variety of waveguide Bragg grating devices. Conventional waveguide Bragg grating device is meant to provide coupling between two oppositely propagating modes to generate narrow stopband and passband in the transmission or reflection spectra. While CDC introduces coupling between modes in different waveguides, therefore, the passband is generated at the output of another waveguide instead of the input of the same waveguide. The design of CDC mainly consists of two parts: 1. Design of the two waveguides so that phase matching takes place between desired modes. 2. Design of the gratings for optimized performance indicators including bandwidth, peak value, sidelobe suppression ratio, Free-Spectral-range (FSR) etc. The coupling occurs specifically between the forward propagating mode in the input waveguide and the backward propagating mode in the coupling waveguide when the phase matching condition is met:

$$\beta_1 + \beta_2 = \frac{2n_{eff1}}{\lambda_0} + \frac{2n_{eff2}}{\lambda_0} = \frac{2\pi}{\Lambda} \tag{1}$$

Where β_1 and β_2 are propagation constants in two waveguides, λ_0 is the center wavelength of the contra-coupling, Λ refers to the grating pitch. The grating will also inevitably cause intra-waveguide reflections when the condition is met:

$$2\beta_i = 2\frac{2n_{effi}}{\lambda_i} = \frac{2\pi}{\Lambda} \tag{2}$$

where i=1 or 2. In previous work, the realized CDC consists of two identical waveguides[18]. Therefore, the coupling takes place between the forward propagating mode to backward propagating modes in both waveguides, resulting in strong back reflections and high insertion loss. To tackle this issue, we use asymmetric waveguides for realizing CDC as shown in Fig. 3(b). The two waveguides are denoted as input and contra-couple waveguide, respectively. The asymmetrical waveguide setting in our design results in a significant difference between the contra-coupling wavelength and the wavelengths at which intra-waveguide reflections occur. The main design efforts are to find the widths of two waveguides at a given grating period Λ to make the intra-waveguide coupling wavelengths λ_i and inter-waveguide coupling wavelength λ_0 as distinct as possible. We have set the pitch Λ to be 305nm, which ensures that the contra-coupling takes place in the C-band. The simulated the transmission spectra, contra-coupling spectra, and intra-waveguide reflection spectra for two different waveguide width configurations: (0.55μm, 0.45μm) and (0.6μm, 0.4μm) are given in Fig, 3(c). Clearly, the distance between contra-coupling wavelength and intra-waveguide reflecting wavelength is proportional to the difference in two waveguide widths. We have specifically chosen the waveguide width to be (0.6μm, 0.4μm) to ensure an adequate separation between the intra-waveguide reflections and the inter-waveguide coupling. This enables reliable contra-coupling of the light and ensures that it either undergoes contra-coupling or propagates towards the output without interference from unwanted reflections.
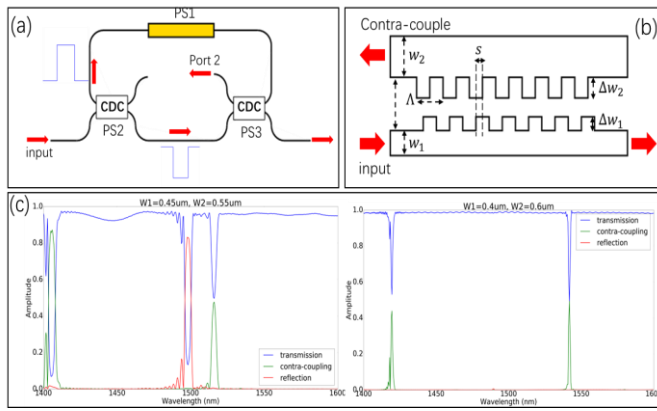
Fig. 3 (a) structure of the narrowband MZI and (b) structure of the asymmetric contra-DC. (c) simulated spectra at different waveguide widths.
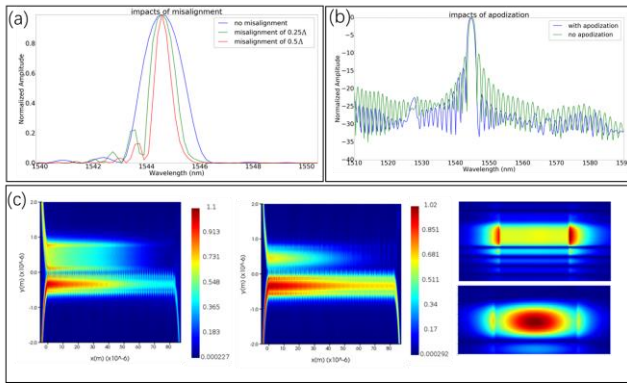

Fig. 4 (a) simulated impacts of the misalignment. (b) simulated impacts of apodization. (c) simulated field distribution and mode profile of the contra-coupling and intra-waveguide reflection conditions.

To achieve a narrow bandwidth for the contra-coupling spectrum, it is necessary to have a weak coupling strength in the grating. The coupling strength is typically determined by the modulation depth of a conventional width-modulated Bragg grating. However, fabrication limitations impose a minimum value for the modulation depth, which can result in undesirably wide coupling bandwidths. In previous studies, cladding modulation was used to ensure a weak coupling strength. However, this approach often requires a long device length and results in low tuning efficiency. In this work, we introduce complementary lateral-misalignment modulation (CLMM) to a conventional width-modulated grating to effectively suppress the coupling strength, as illustrated in Figure 3(b). The modulation depths for the narrow and wide waveguides are set to Δw_1 =40nm and Δw_2 =60nm, respectively, to maintain relatively equal coupling strengths. By increasing the misalignment between the upper and lower gratings, the coupling strength weakens, leading to a narrower bandwidth. In our case, we set the lateral misalignment to be 0.5Λ. Figure 4(a) illustrates the simulated results for different misalignment values, showing that a misalignment of 0.5Λ results in a bandwidth of approximately 0.5nm. To further suppress sidelobes in the spectrum, we apply apodization to the coupling strength. Since achieving a small modulation depth can be challenging, we instead apply apodization to the gap between the two waveguides. This apodization is implemented using a Gaussian profile, where the gap between the waveguides is defined as the parameter for the apodization function:

$$G(z) = G_{min} + H\left[1 - \exp\left(\frac{-\alpha(z - 0.5L)^2}{L^2}\right)\right] \qquad (3)$$

Where G_{min}, H, α and L refer to the minimum gap, apodization amplitude, apodization coefficient and length of the grating, respectively. Fig. 4(b) plots the simulated results with and without apodization. G_{min} is set to be 0.3um, H is 0.15um, α is 2.5 and L is ~240um, which is three times shorter than previous study.[18] The field distribution and mode profile of the final device is plotted in Fig. 4(c). Clearly, at the contra-coupling wavelength, the mode is the second higher TE mode, while at the intra-waveguide reflections, it is the fundamental TE mode.

3. Experimental results

We design a MZI consisting of two aforementioned CDCs as splitter and combiner. The device is fabricated on a 220nm thick silicon wafer using ebeam lithography. Fiber/chip coupling is realized using vertical grating couplers. The device is measured using Agilent 8164B Lightwave measurement system with tunable light source covering 1480nm till 1580nm. The microscopic and SEM images of the device are given in Fig. 5(a). The MZI contains three integrated phase shifters (PS). PS1 is to tune the relative phase change between its two arms, so that the extinction ratio of the notch will be modified, while the wavelength of the notch will remain constant. The PS2 and PS3 are used to tune the center wavelength of the two CDC, so that the center wavelength of the notch would be modified. Besides, these two phase shifters can be used to compensate the spectrum shift of the CDC caused by fabrication variations in the waveguide width and grating periods.
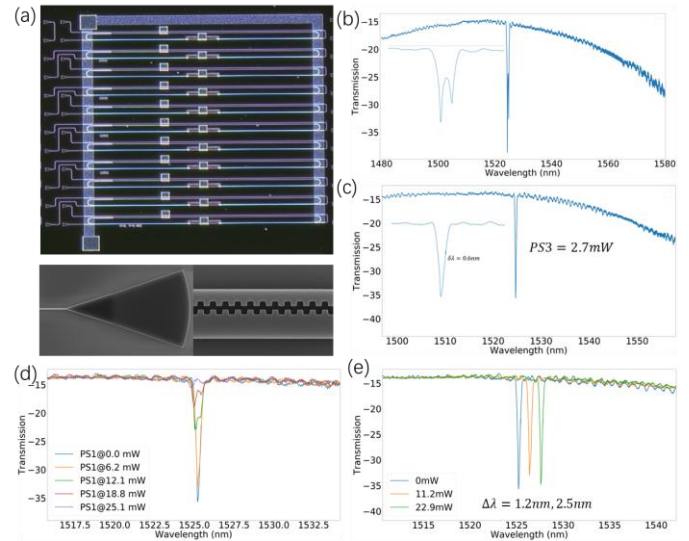

Fig.5 (a) microscopic and SEM images of the fabricated device. (b) static measurement of the MZI. Splitting is present due to misalignment of the passbands of two CDCs. (c) Tuning PS2 or PS3 can eliminate the splitting. (d) Tuning PS1 can effectively tune the transmission of the notch without affecting the rest span. (e) Tuning PS2 and P3 simultaneously can shift the center wavelength of the notch.

First of all, we measure the static transmission spectrum of the MZI. Clearly, a single narrow notch within 100nm span is observed as evident in Fig. 5(b). The splitting is due to the fact that the passbands of the two CDCs are slightly misaligned due to fabrication variations. By tuning PS2 or PS3, the splitting will disappear as shown in Fig. 5(c). The bandwidth is about 0.6nm, which is in good consistency with simulations and has a 4-fold improvement upon the previous work[18]. Next, we show the independent tunability of the transmission coefficient at the center wavelength using PS1. The

results shown in Fig. 5(d) confirms that only the transmission of the notch would be modified, the rest span remains constant during the tuning. Moreover, from the purple line in Fig. 5(d), where the notch is completely eliminated, we could observe that the insertion loss at the center wavelength is negligible. 25mW would change the transmission from 0 to -22dB. The limitation of the maximum extinction ratio is caused by fabrication variations in the peak value of the CDC. If the peak value is closer to 0.5, the extinction ratio can be further improved. Finally, we demonstrate the tunability of the center wavelength by tuning PS2 and PS3 simultaneously. As plotted in Fig. 5(e), the tuning efficiency is about 9.2mW/nm. As we're using thermos-optic effect for the on-chip phase shifters, the tuning speed is in the scale of us, however, our device can also be high-speed modulated once phase shifters based on free-carrier-dispersion effect or electrically reprogrammable transparent phase change materials are used[21].
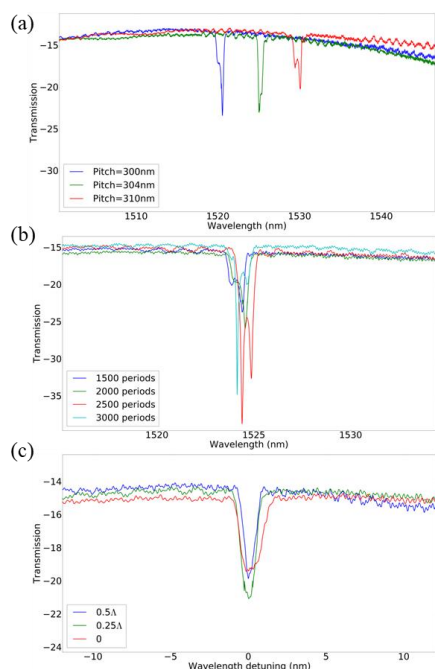

Fig.6 Measured transmission spectra with varying grating pitch of the CDCs (a), varying numbers of gratings (b) and varying lateral misalignment of the CDCs (c).

We also performed additional experimental characterizations of multiple devices with varying CDC parameters to understand the impacts of different parameters including grating pitch, number of gratings and lateral misalignment. The dependency of grating pitch is shown in Fig. 6(a), as expected, the center wavelength can be efficiently shifted towards longer wavelength by increasing grating pitch. The impacts of total grating numbers are plotted in Fig. 6(b). When the total periods grow from 1500 to 2500, the extinction ratio of the notch exhibits a clear improvement, indicating the coupling ratio is stronger and closer to 0.5. While further increasing the grating number to 3000 we notice a drop in the extinction ratio, as now the coupling ratio surpasses 0.5. The impacts of later misalignment are provided in Fig. 6(c), which is in good consistency with simulations as increasing the misalignment could effectively reduce the overall bandwidth.

4. conclusion

In this paper, we successfully demonstrated a narrow notch filter with 0.6nm bandwidth and an ultra-wide FSR over 100nm. The bandwidth can be further reduced by using multimodal waveguide grating or by reducing the duty cycle of the grating. Additionally its extinction ratio, namely the transmission at the center wavelength of the notch can be independently tuned without affecting the rest span. The device is a MZI with narrowband CDCs serving as the splitter and combiner. Each CDC has a length around 240um. Experimental results demonstrate that 25mW power consumption would change the transmission from 0 to -22dB. The center wavelength of the notch can also be tuned with an efficiency of 9.2mW/nm. Our device can be developed towards optical sensors with broad operation range and high sensitivity, programmable photonic circuits, single-mode high speed modulators etc.

Disclosures. The authors declare no conflicts of interest.

Data availability. Data underlying the results can be obtained upon request from the corresponding author.

References

1. L. Zhuang, et al., "Novel microwave photonic fractional Hilbert transformer using a ring resonator-based optical all-pass filter," Optics express **20**, 26499-26510 (2012).
2. U. Kurokawa, et al., "Filter-Based Miniature Spectrometers: Spectrum Reconstruction Using Adaptive Regularization," IEEE Sensors Journal **11**, 1556-1563 (2011).
3. H. Shen, et al., "Eight-channel reconfigurable microring filters with tunable frequency, extinction ratio and bandwidth," Optics express **18**, 18067-18076 (2010).
4. Z. Wang and S. Fan, "Compact all-pass filters in photonic crystals as the building block for high-capacity optical delay lines," Physical Review E **68**, 066616 (2003).
5. C. Madsen, et al., "Integrated all-pass filters for tunable dispersion and dispersion slope compensation," IEEE Photonics Technology Letters **11**, 1623-1625 (1999).
6. C. Sun, et al., "Tunable narrow-band single-channel add-drop integrated optical filter with ultrawide FSR," PhotoniX **3**, 12 (2022).
7. A. Li and W. Bogaerts, "Experimental demonstration of a single silicon ring resonator with an ultra-wide FSR and tuning range," Optics letters **42**, 4986-4989 (2017).
8. Y. Long and J. Wang, "Optically-controlled extinction ratio and Q-factor tunable silicon microring resonators based on optical forces," Scientific Reports **4**, 5409 (2014).
9. W. Bogaerts, et al., "Programmable photonic circuits," Nature **586**, 207-216 (2020).
10. J. Capmany, et al., "The programmable processor," Nature Photonics **10**, 6-8 (2016).
11. L. Zhuang, et al., "Programmable photonic signal processor chip for radiofrequency applications," Optica **2**, 854-859 (2015).
12. E. Sánchez, et al., "Simulation of Highly Coupled Programmable Photonic Circuits," Journal of Lightwave Technology **40**, 6423-6434 (2022).
13. D. Pérez-López, et al., "Multipurpose self-configuration of programmable photonic circuits," Nature communications **11**, 6359 (2020).

14. A. Li, et al., "An integrated single-shot spectrometer with large bandwidth-resolution ratio and wide operation temperature range," PhotoniX **4**, 29 (2023).

15. P. Dong, et al., "Thermally tunable silicon racetrack resonators with ultralow tuning power," Optics express **18**, 20298-20304 (2010).

16. H. Qiu, et al., "A continuously tunable sub-gigahertz microwave photonic bandpass filter based on an ultra-high-Q silicon microring resonator," Journal of Lightwave Technology **36**, 4312-4318 (2018).

17. S. Zheng, et al., "A single-chip integrated spectrometer via tunable microring resonator array," IEEE Photonics Journal **11**, 1-9 (2019).

18. J. A. Davis, et al., "Novel spectral-shaping building block: a narrowband Mach–Zehnder interferometer," Photonics Research **8**, 1059-1063 (2020).

19. W. Shi, et al., "Silicon photonic grating-assisted, contra-directional couplers," Optics express **21**, 3633-3650 (2013).

20. W. Shi, et al., "Ultra-compact, flat-top demultiplexer using anti-reflection contra-directional couplers for CWDM networks on silicon," Optics express **21**, 6733-6738 (2013).

21. C. Ríos, et al., "Ultra-compact nonvolatile phase shifter based on electrically reprogrammable transparent phase change materials," PhotoniX **3**, 26 (2022).